Magdalena Matusiak-Małek
Institute of Geological Sciences, University of Wrocław,
corresponding author: magdalena.matusiak@ing.uni.wroc.pl

Jacek Puziewicz
Institute of Geological Sciences, University of Wrocław

Theodoros Ntaflos
Department of Lithospheric Sciences, University of Vienna

Origin of intergranular aggregates in mantle xenoliths from Krzeniów basanite

Abstract

The upper mantle harzburgite and dunite xenoliths occurring in the Miocene basanite from Krzeniów (Lower Silesia, SW Poland) contain abundant (up to 16 vol. %) fine-grained mineral aggregates. The xenoliths consist of olivine I, ortho- and clinopyroxene I and spinel I. The aggregates are formed of clinopyroxene II, olivine II ± spinel II ± glass ± feldspar ± sulfides (Ni-pyrrhotite, pentlandite and chalcopyrite). The aggregates occur as intergranular "patches" or envelop grains of orthopyroxene I. They originated due to the reaction of primary harzburgite/dunite phases with S-bearing alkaline silicate melt. The reaction led to changes of chemical composition of clinopyroxene I olivine I and spinel I or to crystallization of new phases (feldspar, sulfides). Apart from aggregates, the xenoliths are cut by scarce veinlets filled mostly with feldspar and apatite. Those veinlets were formed due to infiltration of Fsp-bearing P-rich melt after xenoliths entrainment into host magma. Lack of well-developed host basanite/xenolith reaction zones suggest short but legible contact between them.

Streszczenie

Harzburgitowe i dunitowe ksenolity skał górnego płaszcza występujące w bazanicie z Krzeniowa (Dolny Śląsk, SW Polska) zawierają liczne (do 16 % obj.) drobnoziarniste agregaty międzyziarnowe. Ksenolity zbudowane są z oliwinu I, orto- i klinopiroksenu I oraz spinelu I. Agregaty zbudowane są z klinopiroksenu II, oliwinu II ± spinelu II ± szkliwa ± skalenia ± siarczków (Ni-pirotyn, pentlandyt, chalkopiryt). Agregaty występują jako „kieszenie" międzyziarnowe lub tworzą otoczki dookoła ziaren ortopiroksenu I. Agregaty powstały w wyniku reakcji pierwotnych faz harzburgitu/dunitu z alkalicznym stopem krzemianowym bogatym w S. Reakcja doprowadziła do zmian składu chemicznego klinopiroksenu I, oliwinu I i spinelu I, a także do krystalizacji nowych faz (skaleń, siarczki). Wydarzenie to miało miejsce krótko przed wprowadzeniem ksenolitów do wznoszącego

się bazanitu. Oprócz agregatów w ksenolitach z Krzeniowa występują nieliczne żyłki zbudowane ze skalenia i apatytu. Żyłki te powstały w wyniku infiltracji przez skalenionośny krzemianowy stop bogaty w P. Brak dobrze rozwiniętych stref kontaktowych pomiędzy ksenolitami a bazanitem z Krzeniowa sugeruje ich krótką, ale wyraźną interakcję.

Keywords: mantle xenolith, Sudetes, intergranular aggregates, melt infiltration

1. Introduction

Fragments of upper mantle rocks are being extracted from the lithospheric mantle by ascending alkaline and kimberlitic magmas. While brought to Earth's surface as peridotite xenoliths, they provide a source of information on mantle composition, structure and evolution. Olivine, clino- and orthopyroxene as well as Al-rich, pressure dependent phases forming peridotite carry majority of the information. Many of mantle xenoliths described in literature contain variable amounts of fine-grained, glass or feldspar bearing intergranular aggregates ("patches," "pools," "pockets") which also constitute an important, often underestimated source of data about mantle composition and evolution.

Despite significant number of publications dedicated to the aggregates, their origin is still a question of debate. Their presence may be related to direct infiltration of host magma during ascend (Bonadiman et al. 2011) or host-related melts at mantle depths (Shaw and Klügel 2002) or they can be remnants of another metasomatic melts (Coltorti et al. 2000). The intergranular pockets may be formed also as a result of in situ peridotite melting due to decompression or heating (Yaxley and Kamenetsky 1999) or breakdown of peridotite due to reaction with infiltrating melts/fluids (Aliani et al. 2009; Shaw 1999; Shaw and Klügel 2002). Fine-grained intergranular patches occurring in Polish xenoliths are interpreted as an effect of host magma infiltration shortly before eruption (Lutynia, Lądek Zdrój vicinity; Matusiak-Małek et al. 2010) or infiltration of alkaline silicate melts at mantle depths (Księginki, Lubań vicinity; Puziewicz et al. 2011). Typical aggregate is formed of olivine, clinopyroxene, opaques and variable amounts of other phases (amphibole, phlogopite, rhönite, carbonates, zirconolite and others); they never contain orthopyroxene (Coltorti et al. 2000). Great majority of the pockets described worldwide are glass bearing, feldspar-bearing ones occur scarcely (Matusiak-Małek et al. 2010; Su et al. 2010).

The main goal of this study is to give a consistent description of intergranular aggregates in xenoliths from Krzeniów basanites (SW Poland). On a base of optical observations and in situ chemical analyses we have established the possible origin of fine-grained intergranular aggregates in upper mantle xenoliths beneath northern margin of Bohemian Massif.

2. Regional settings

Alkaline volcanic rocks of Cenozoic age are widespread to the north of the Alpine chain forming the Cenozoic Central European Volcanic Province (CEVP; Figure 1).

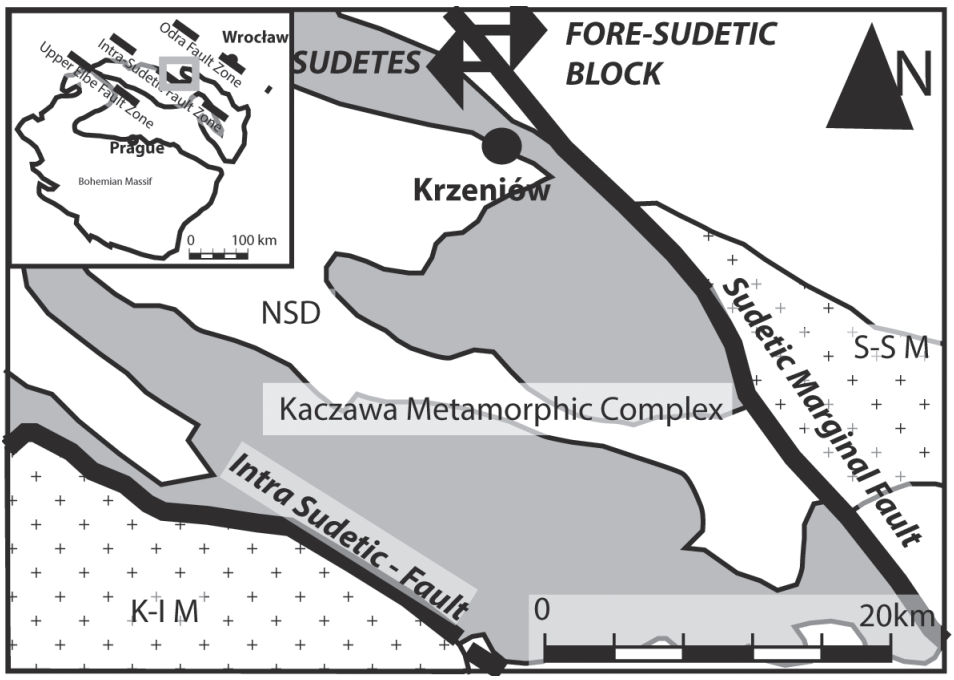

Figure 1. Location of the Krzeniów basanite relative to neighboring geological units. K-I M — granitic Karkonosze-Izera Massif; S-S M — granitic Strzegom-Sobótka Massif; NSD — North Sudetic Depression. Modified after (Albrycht et al. 2006)

The volcanic activity was triggered by intraplate compressional stresses related to the African and Eurasian plate collision (Dèzes et al. 2004). The Cenozoic alkaline rock vary in composition from silica poor (leucitites, nephelinites, etc.) to silica enriched (trachytes; Meyer and Foulger 2007).

Volcanic activity in the eastern branch of CEVP (SW Poland) persisted from 60 to ca. 4 Ma with main phases in late Oligocene (30–26 Ma) and early Miocene (23–15 Ma, K-Ar datings; Birkenmajer and Pécskay 2002; Birkenmajer et al. 2004b, 2007; Birkenmajer et al. 2002). Majority of the over-three-hundreds outcrops is located in Lower Silesia region and concentrate in four volcanic fields: Lubań–Frydlant, Złotoryja–Jawor, Niemcza–Strzelin, Lądek Zdrój; only Niemodlin concentration is located in Opole Silesia region. The composition of alkaline volcanic rocks from SW Poland follows the compositional variability of the whole

CEVP, but alkali basalts, basanites and nephelinites are the most common (Birkenmajer et al. 2004a; Ladenberger 2006; Wierzchołowski 1993).

The Krzeniów (Wilków village) volcanic plug is located in the Złotoryja-Jawor volcanic field (Birkenmajer et al. 1970), in the vicinity of Złotoryja city. The occurrence is located in the North-Sudetic Depression and is underlain by Cretaceous limestones and sandstones (Albrycht et al. 2006). The K-Ar datings of basanite showed 19.57 ± 0.79 to 18.72 ± 0.81 Ma (Birkenmajer et al. 2007).

The lavas from Krzeniów contain small amounts of mafic and ultramafic xenoliths. The study by Białowolska (1993) showed that ultramafic xenoliths are of mantle origin, while mafic rocks are cumulates of host magma. Bakun-Czubarow and Białowolska (2003) established the equilibration temperatures for all the Złotoryja-region gabbroic xenoliths for 1100°C (under pressure of 1.0 GPa). Matusiak-Małek (2010) suggested that harzburgites and dunites occurring in Krzeniów record at least one melting event followed by two episodes of cryptic metasomatism: (1) by carbonatitic melt and by (2) alkaline melt. The last metasomatic event, probably of regional range, was triggered by a Fe-rich metasomatic agent.

Petrographic descriptions of Krzeniów ultramafic xenoliths by Białowolska (1993) showed that intergranular, fine-grained olivine-clinopyroxene-spinel-glass "blebs" constitute up to 10% of xenoliths' volume. The author interpreted the "blebs" to originate by incongruent melting of orthopyroxene (ibid.). Bakun-Czubarow and Białowolska (2005) concluded that intergranular aggregates from the Złotoryja vicinity xenoliths are products of in situ melting of wall-rock peridotite followed by fast crystallization after entrapment by the basanitic magma while Matusiak-Małek (2010) tentatively interpreted the aggregates from Krzeniów as a result of magma infiltration and melt-induced orthopyroxene decomposition.

3. Analytical methods and terminology

The data presented in this article are based on a study of 19 xenoliths collected in an active Krzeniów basalt quarry belonging to "Przedsiębiorstwo Górniczo-Produkcyjne BAZALT S.A." Xenoliths were cut, sliced and polished into 150 μm thick sections at the University of Wrocław. Modal composition of xenoliths was estimated by using a digital method of image analysis by Higgins (2000) on high-resolution scans of one thick section per xenolith.

The electron microprobe analyses were conducted on Cameca SX-100 at the Department of Lithospheric Research at the University of Vienna, Austria, under standard conditions (acceleration voltage 15 kV, sample current 15 nA, counting times 10 or 20 s, natural silicates and synthetic oxides as standards). PAP correction procedure was applied. Counting times were lengthened to improve detection limits for Ni and Ca.

The pyroxene nomenclature after Morimoto (1989) was used. Spinel compositions were calculated on the basis of three cations and the proportions of Fe^{3+} and Fe^{2+} were determined on the basis of charge balance (Deer et al. 1993). Acronym "a.pfu." stands for atoms per formula unit. The cr-number or cr# denotes the atomic ratio of Cr/(Cr+Al), while mg-number or mg# stands for atomic $Mg/(Mg+Fe^{tot})$. Forsterite (Fo) content in olivine is calculated as $Mg/(Mg+Fe^{tot})*100$ per olivine formula unit. Mineral abbreviations are: Ol (olivine), Opx (orthopyroxene), Cpx (clinopyroxene), Spl (spinel), Afs/Pl (alkali feldspar/plagioclase), Ap (apatite), Po (pyrrhotite) and Pn (pentlandite).

4. Petrography and chemical composition

The Krzeniów xenoliths are formed of two generations of minerals: primary, xenolith-forming (denoted as I) and secondary (denoted as II) forming the fine-grained integranular aggregates. Detailed data on chemical composition of peridotite-forming minerals is given in Matusiak-Małek (2010).

4.1. Xenoliths

4.1.1. Peridotite-forming minerals

The Krzeniów basanite contains scarce spinel harzburgite/dunite xenoliths, usually up to 4 cm across with clinopyroxene content from 0 to 3.9 vol.%. The textures of peridotitic xenoliths vary from protogranular to porphyroclastic (sensu Mercier and Nicolas 1975). Representative chemical analyses of peridotite-forming minerals are given in Table 1.

Chemical composition of olivine and orthopyroxene classify the Krzeniów xenolith suite into two groups: group A — with iron content typical for Phanerozoic mantle (Griffin et al. 1999) and group B — with elevated iron content due to Fe-metasomatism (Matusiak-Małek 2010).

Olivine I forms anhedral crystals from 1 to 5 mm with the largest displaying kink banding. The group A ($Fo_{90.4-91.7}$) olivine I is chemically homogeneous within a single xenolith, while group B olivine I ($Fo_{88.2-89.8}$) is heterogeneous within a single xenolith. The NiO content in groups A and B is ≥ 0.30 wt.%. The Ca content in olivine from both the groups is typically below 700 ppm.

Orthopyroxene I occurs as anhedral grains from 2 to 5 mm with abundant exsolution lamellae of clinopyroxene. Composition of orthopyroxene I varies from enstatite, through Cr- enstatite to Al, Cr-enstatite. The mg — number of orthopyroxene I is similar in all the group A xenoliths (0.913–0.921), while in group B its range is wider (0.899–0.920).

Table 1. Representative analyses and structural formulae (Ol : O^{2-} = 4; Cpx, Opx: O^{2-} = 6, Spl : K = 3) of Krzeniów xenolith-forming minerals, after (Matusiak-Małek 2010)

No.	1	2	3	4	5	6	7	8	9	10	11	12	13	14	15	16	17
Mineral	Ol	Ol	Ol	Ol	Opx	Opx	Opx	Opx	Cpx	Cpx	Cpx	Cpx	Cpx	Spl	Spl	Spl	Spl
Group	A	A	B	B	A	A	B	B	A	A	A	B	B	A	A	A	B
SiO_2	41.580	41.496	40.204	40.962	57.150	56.561	56.989	56.868	54.260	53.580	53.822	54.520	53.907	0.004	0.022	0.058	0.093
TiO_2	—	0.012	0.005	0.008	0.020	0.017	0.036	0.030	0.040	0.050	0.000	0.009	0.015	0.061	0.000	0.123	14.452
Al_2O_3	0.000	0.014	0.024	0.000	1.480	2.544	1.423	0.958	1.410	2.900	1.829	1.892	1.764	29.541	36.910	29.388	51.397
Cr_2O_3	0.000	0.020	0.120	0.014	0.220	0.639	0.368	0.352	0.410	0.870	1.227	1.395	1.234	35.780	29.478	37.320	19.596
FeO*	8.330	8.619	8.072	11.113	5.620	5.496	7.394	6.465	1.880	2.470	2.089	2.445	3.221	18.686	15.060	13.483	0.236
MnO	0.090	0.116	0.123	0.188	0.150	0.112	0.176	0.150	0.010	0.070	0.051	0.059	0.106	0.102	0.115	0.115	0.094
NiO	0.420	0.349	0.320	0.372	0.090	0.110	0.080	0.108	0.040	0.020	0.037	0.053	0.059	0.165	0.249	0.165	12.458
MgO	50.510	49.881	50.238	48.755	35.270	34.316	33.426	34.844	17.760	16.810	17.100	17.026	16.667	15.234	17.111	16.508	0.012
CaO	0.030	0.053	0.134	0.035	0.390	0.779	0.637	0.507	23.860	22.390	21.900	21.937	21.823	—	—	—	—
Na_2O	—	—	—	0.013	0.010	0.049	0.048	0.053	0.260	0.830	0.978	0.997	1.009	0.001	0.016	0.042	0.000
Total	100.960	100.579	100.158	100.699	100.400	100.623	100.577	100.335	99.930	99.990	99.033	100.333	99.815	99.574	98.954	97.151	98.338
Si^{+4}	1.004	1.007	0.983	1.006	1.954	1.935	1.965	1.952	1.965	1.939	1.964	1.968	1.960	0.000	0.001	0.002	0.000
Ti^{+4}	0.000	0.000	0.000	0.000	0.001	0.000	0.001	0.001	0.001	0.001	0.000	0.000	0.000	0.001	0.000	0.003	0.002
Al^{+3}	0.000	0.000	0.000	0.000	0.060	0.103	0.058	0.039	0.060	0.124	0.079	0.080	0.076	1.027	1.240	1.034	0.550
Cr^{+3}	0.000	0.000	0.000	0.000	0.006	0.017	0.010	0.010	0.012	0.025	0.035	0.040	0.035	0.834	0.664	0.881	1.311
Fe^{+2}	0.168	0.175	0.227	0.212	0.161	0.157	0.213	0.186	0.057	0.075	0.064	0.074	0.098	0.136	0.096	0.079	0.135
Fe^{+3}	0.000	0.000	0.000	0.000	0.000	0.000	0.000	0.000	0.000	0.000	0.000	0.000	0.000	0.325	0.263	0.258	0.394
Mn^{+2}	0.002	0.002	0.004	0.004	0.004	0.003	0.005	0.004	0.000	0.002	0.002	0.002	0.003	0.003	0.003	0.003	0.006
Ni^{+2}	0.008	0.007	0.007	0.007	0.002	0.003	0.002	0.003	0.001	0.001	0.001	0.002	0.002	0.004	0.006	0.004	0.002
Mg^{+2}	1.817	1.805	1.777	1.769	1.798	1.750	1.718	1.783	0.959	0.907	0.930	0.916	0.904	0.670	0.727	0.735	0.599
Ca^{+2}	0.001	0.001	0.001	0.001	0.014	0.029	0.024	0.019	0.926	0.868	0.856	0.848	0.850	0.000	0.000	0.000	0.000
Na^{+1}	—	—	0.0001	—	0.001	0.000	0.003	0.004	0.018	0.058	0.069	0.070	0.071	0.000	0.000	0.000	0.000
Total	3.000	3.000	3.000	3.000	4.000	3.997	3.999	4.000	4.000	4.000	3.999	3.999	3.999	3.000	3.000	3.000	3.000
Fo[%]-/mg#	91.5	91.2	88.7	89.3	0.918	0.918	0.890	0.906	0.944	0.924	0.936	0.925	0.902	0.592	0.734	0.686	0.603
Ca [ppm]	214	249	250	343	—	—	—	—	—	—	—	—	—	—	—	—	—
cr#	—	—	—	—	—	—	—	—	—	—	—	—	—	0.448	0.349	0.460	0.705

*total iron

Clinopyroxene I forms anhedral crystals from 200 to 850 μm; clinopyroxene in only two of the 19 xenoliths contains lamellae of orthopyroxene and spinel. Chemical composition of group A clinopyroxene I varies from diopside (mg# = 0.936–0.945), through Cr-diopside (mg# = 0.932–0.936) to Al, Cr-diopside (mg# = 0.930 to 0.918). In group B clinopyroxene I has composition of Cr-diopside (mg# = 0.903–0.924).

Oval to elongated crystals of spinel I (200–350 μm long) occur scarcely in the majority of the xenoliths; uneven-margined spinel I occurs in some of the intergranular aggregates, however its size and composition suggests it to be a primary phase. Composition of spinel I in clinopyroxene-bearing group A xenoliths is variable but generally characterized by low (0.348–0.640, scarcely up to 0.755) cr-number, while Cr# in spinel I in clinopyroxene- free xenoliths is 0.511–0.692. The mg-number in group A spinel I is 0.511–0.708. The composition of spinel I occurring in group B xenoliths is scattered respect to mg-number (0.506–0.647), while cr-numbers are high (0.598–0.705).

4.1.2. Intergranular aggregates

Fine-grained intergranular aggregates form 0.7 to 17 vol. % of Krzeniów xenoliths (Figure 2a). No visible basanite infiltration can be followed from aggregate to the basanite/xenolith contact but veinlets (from first to 200 μm wide) filled with feldspar, apatite and spinel (Figure 2b) crosscut some of the xenoliths.

The intergranular aggregates are formed of olivine II + clinopyroxene II ± spinel II + alkali feldspar/ternary feldspar/plagioclase/glass ± sulfides ± apatite. The aggregates may be elongated along grain boundaries, oval or angular. The elongated ones have the length of the neighboring grains and are usually ca. 100 μm wide, while longer axes of oval and angular ones are from 150 to over 1 000 μm. Contacts of aggregates with olivine I are uneven or lobate but well defined. Orthopyroxene I grains (bordering an aggregate and some of crystals without direct contact with aggregate) are enveloped by thin (~20μm) zones of vermicular to angular clinopyroxene II ± olivine II ± glass (Figure 2c); occasionally the orthopyroxene I/aggregate contact is developed to mixture of vermicular clinopyroxene II and olivine II ± glass (Figure 2d). In one grain (among all the studied xenoliths) of orthopyroxene I a process of decomposition to clinopyroxene II + olivine II and glass is preserved (Figure 2e). Clinopyroxene I scarcely contacts with an aggregate, but if so, the crystal margins are zoned. Sulfides are present in variable amounts (from single grain to few tens of grains) in aggregates in both groups (A and B) of xenoliths. Laths of feldspar are occasionally parallel to each other or display fan-like structure while in only one of the xenoliths subhedral crystals of clinopyroxene II are parallel (Figure 2f).

Aggregates containing alkali/ternary feldspar/plagioclase may coexist in one xenolith with glass-bearing aggregates. Distinction between feldspar and glass

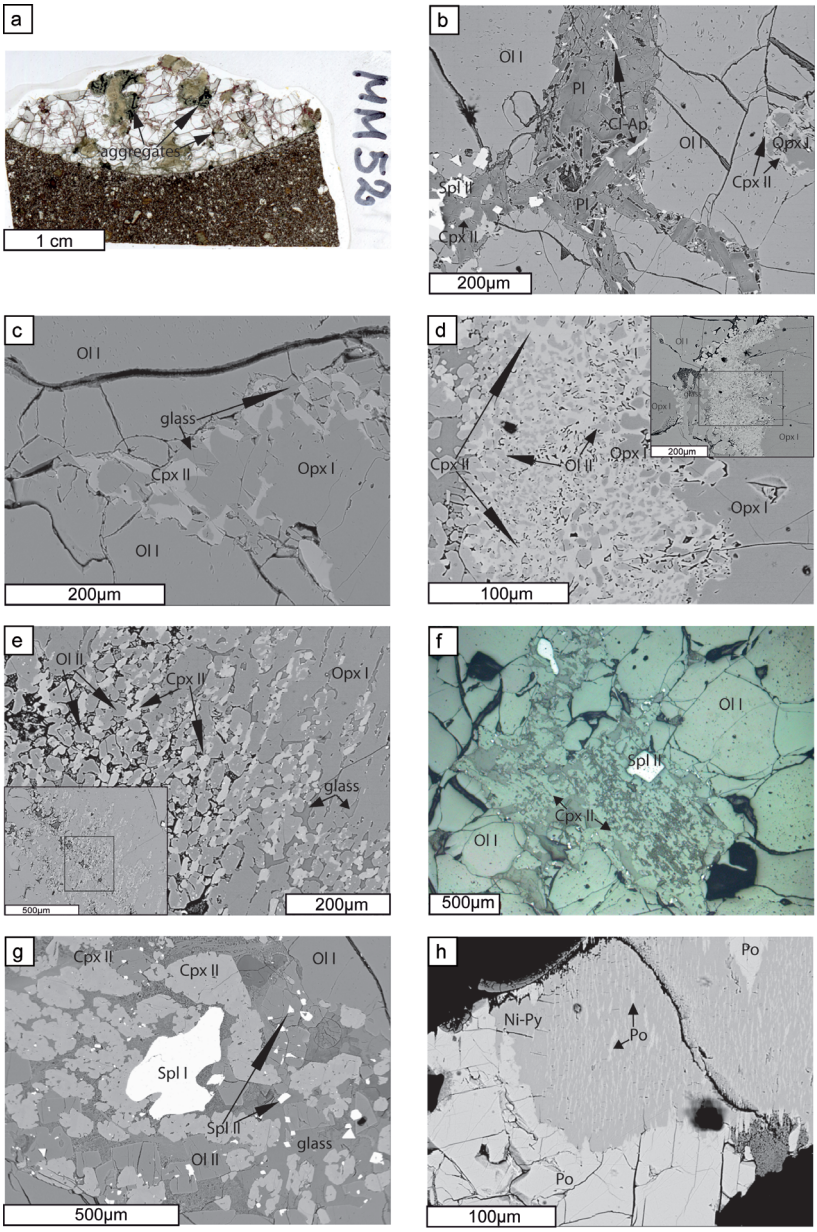

Figure 2. Texture of peridotite and interstitial fine-grained aggregates in Krzeniów xenoliths. (a) Fine-grained intergranular aggregates in Krzeniów xenolith. Xenolith MM52 with 16 vol.% of aggregates. Scan of thick section. (b) Veinlet in xenolith MM55, BSE image. (c) Clinopyroxene II and glass rimming orthopyroxene I. Xenolith MM58, BSE image. (d) Reaction zone around orthopyroxene I developed into mixture of olivine and clinopyroxene. Inset shows enlargement of the structure. Xenolith MM50, BSE image. (e) Decomposition of orthopyroxene I. Inset shows enlargement of the reaction. Xenolith MM50, BSE image. (f) Parallel crystals of clinopyroxene II. Xenolith MM61, reflected light. (g) Texture of fine-grained aggregates. Xenolith MM47, BSE image. (h) Sulfide in intergranular aggregate. Xenolith MM72, BSE image

is problematic due to: (1) small size and similar appearance in BSE image, (2) devitrification processes, (3) similar textural position. Thus we call feldspar (plagioclase, alkali feldspar or ternary feldspar) all the intra-aggregate intergranular objects without isotropic characteristic (in polarized light) and not containing significant amount of iron and magnesium (e.g. Coltorti et al. 2000; Dawson 2002). Plagioclase usually forms eu- to subhedral 20–150 μm long laths of composition $An_{23-59}Or_{1-10}Ab_{37-65}$ with scarce transitions to ternary feldspar. Ternary feldspar ($An_{5-20}Or_{11-30}Ab_{63-68}$) occurs either as subhedral laths or anhedral crystals, while alkali feldspar ($An_{1}Or_{25-54}Ab_{43-73}$) is usually anhedral (Figure 3, Table 2). Composition of aggregate-forming feldspar is not correlated with modal composition of host xenolith nor with composition of peridotite-forming minerals.

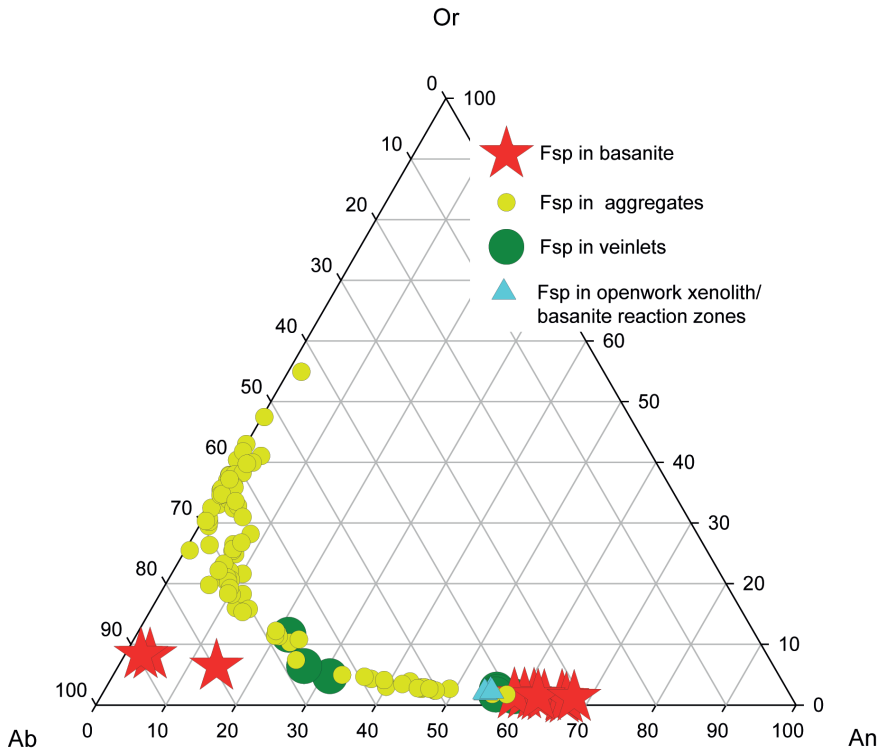

Figure 3. Composition of feldspar from intergranular aggregates, xenolith/basanite reaction zones and host basanite. Data for basanite after (Matusiak-Małek 2010)

Feldspar occurring in veinlets forms eu- to subhedral laths of from 50 to 200 μm wide. Feldspar shows normal chemical zonation: $An_{56-59}Or_{1-3}Ab_{40-42}$ in cores, $An_{22-31}Or_{3-12}Ab_{64-67}$ in rims (Figure 3, Table 2).

Massive, sometimes slightly cracked and locally devitrified glass occurs in interstices in some of the aggregates. It is always associated with feldspar-bearing aggregates. Glass in aggregates occurring without visible contact with orthopyroxene has composition of trachyandesite, scarcely dacite/trachydacite (mg# =

Table 2. Representative analyses and structural formulae (O^{2-} = 6) of feldspar

No.	1	2	3	4	5	6	7	8	9	10	11	12	13	14	15	16	17	18
Type of feldspar	K-Fsp	K-Fsp	K-Fsp	K-Fsp	Pl	Pl	Pl	Pl	Pl	T Fsp	T Fsp	T Fsp	T Fsp	T Fsp	T Fsp	V	V	V
Group of primary grains	A	A	A	B	A	A	B	B	B	A	A	A	A	B	B	B	B	B
SiO_2	66.439	66.200	62.876	66.719	58.091	55.748	55.915	57.616	54.602	68.438	63.493	63.620	64.475	60.771	63.432	61.53	60.684	52.8
TiO_2	0.169	0.200	0.472	0.232	0.072	0.157	0.137	0.143	0.180	0.505	0.139	0.270	0.045	0.196	0.791	0.42	0.363	0.162
Al_2O_3	18.753	18.100	19.988	19.206	25.441	27.579	28.081	26.436	27.662	19.215	21.464	21.480	20.963	23.585	21.513	23.82	24.306	29.519
Cr_2O_3	0.044	0.020	0.004	0.004	0.023	0.107	0.288	0.028	0.000	0.019	0.089	0.080	0.117	0.006	0.037	0.02	0.008	0
FeO*	0.602	0.370	0.235	0.085	0.242	0.284	0.396	0.218	0.223	0.234	0.161	0.170	0.129	0.228	0.252	0.22	0.164	0.273
MnO	0.011	0.010	0.000	0.013	0.000	0.022	0.000	0.005	0.000	0.018	0.023	0.000	0.031	0.000	0.000	0.01	0.033	0.006
NiO	0.000	—	0.007	0.008	0.000	0.008	0.000	0.000	0.001	0.001	0.000	—	0.018	0.000	0.000	0.02	0.04	0.072
MgO	0.115	0.110	0.016	0.012	0.017	0.033	0.086	0.040	0.038	0.045	0.015	0.030	0.009	0.000	0.005	0.01	5.503	12.025
CaO	0.073	0.240	0.514	0.387	6.829	9.716	9.486	7.906	9.599	0.113	1.994	2.690	1.329	4.678	2.079	4.47	7.678	4.464
Na_2O	5.929	5.170	6.664	7.030	7.199	5.701	5.774	6.339	5.659	7.586	8.202	7.970	7.796	7.684	7.704	7.56	1.113	0.243
K2O	8.191	8.350	7.018	6.151	0.868	0.405	0.458	0.697	0.403	5.053	3.369	2.600	3.773	1.790	3.708	1.99	0.05	0.048
Total	100.326	98.770	97.794	99.847	98.782	99.760	100.621	99.428	98.367	101.227	98.949	98.910	98.685	98.938	99.521	100.08	99.942	99.612
Si^{+4}	2.985	3.013	2.899	2.982	2.635	2.518	2.506	2.596	2.501	2.998	2.859	2.857	2.902	2.742	2.844	2.743	2.707	2.401
Ti^{+4}	0.006	0.007	0.016	0.008	0.002	0.005	0.005	0.005	0.006	0.017	0.005	0.009	0.002	0.007	0.027	0.014	0.012	0.006
Al^{+3}	0.993	0.971	1.086	1.012	1.360	1.468	1.483	1.404	1.493	0.992	1.139	1.137	1.112	1.254	1.137	1.252	1.278	1.582
Cr^{+3}	0.002	0.001	0.000	0.000	0.001	0.004	0.010	0.001	0.000	0.001	0.003	0.003	0.004	0.000	0.001	0.001	0.000	0.000
Fe^{+2}	0.023	0.014	0.009	0.003	0.009	0.011	0.015	0.008	0.009	0.009	0.006	0.006	0.005	0.009	0.009	0.008	0.006	0.010
Mn^{+2}	0.000	0.000	0.000	0.000	0.000	0.001	0.000	0.000	0.000	0.001	0.001	0.000	0.001	0.000	0.000	0.000	0.001	0.000
Ni^{+2}	0.000	0.000	0.000	0.000	0.000	0.000	0.000	0.000	0.000	0.000	0.000	0.000	0.001	0.000	0.000	0.001	0.003	0.005
Mg^{+2}	0.008	0.007	0.001	0.001	0.001	0.002	0.006	0.003	0.003	0.003	0.001	0.002	0.001	0.000	0.000	0.001	0.263	0.586
Ca^{+2}	0.004	0.012	0.025	0.019	0.332	0.470	0.455	0.382	0.471	0.005	0.096	0.129	0.064	0.226	0.100	0.213	0.664	0.394
Na^{+1}	0.516	0.456	0.596	0.609	0.633	0.499	0.502	0.554	0.503	0.644	0.716	0.694	0.680	0.672	0.670	0.654	0.063	0.014
K^{+1}	0.469	0.485	0.413	0.351	0.050	0.023	0.026	0.040	0.024	0.282	0.194	0.149	0.217	0.103	0.212	0.113	0.002	0.002
Total	5.005	4.965	5.046	4.984	5.024	5.002	5.007	4.993	5.009	4.952	5.020	4.986	4.987	5.012	5.001	5.000	5.000	5.000
Or	47	51	40	36	5	2	3	4	2	30	19	15	23	10	22	12	6	1
Ab	52	48	58	62	62	50	51	57	50	69	71	71	71	67	68	67	67	40
An	0	1	2	2	33	47	46	39	47	1	10	13	7	23	10	22	27	59

*total iron; K-Fsp — alkali feldspar; Pl — plagioclase; T Fsp — ternary feldspar; V — feldspar in veinlets.

0.309–0.643; Figure 4); content of all the elements vary in wide ranges (Ca = 0.05–1.41 wt.%, Al = 16.80–24.04 wt.%, Ti = 0.04–1.93 wt.%.; Table 3).

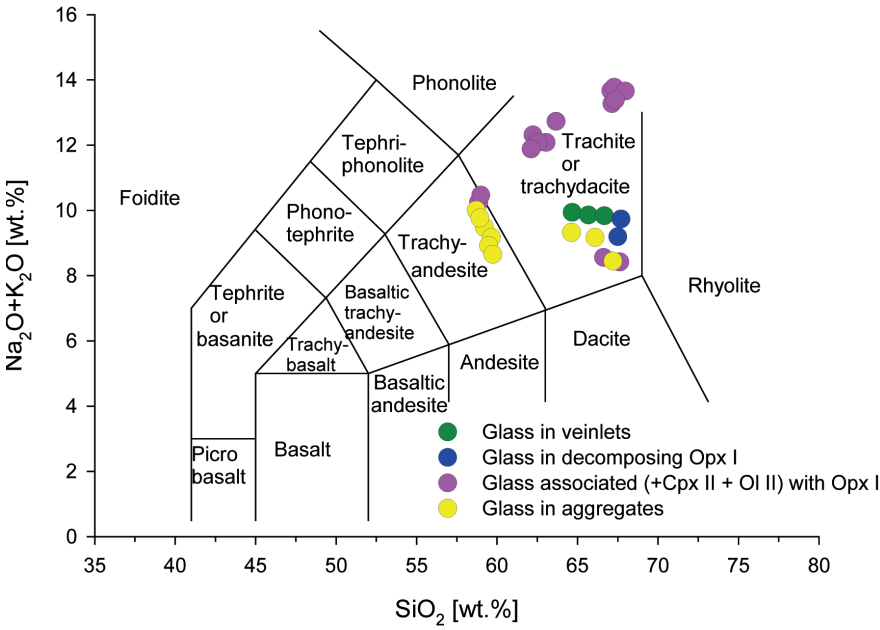

Figure 4. Composition of glass occurring in Krzeniów xenoliths. Diagram after (Le Maitre et al. 1989)

Chemical composition of glass coexisting with clinopyroxene II and olivine II around orthopyroxene I is trachytic/trachydacitic with transition to trachyandesitic (mg# = 0.300–0.478) and is characterized by low Ca content (0.03–0.54 wt.%., Al = 17.91–22.50 wt.%, Ti = 0.19–1.52 wt.%); glass associated with decomposed orthopyroxene I is trachytic/dacitic (mg# = 0.601–0.805) with low amounts of Ca, Al and Ti (0.05–0.07 wt.%, 15.82–16.51 wt.% and 0.03–0.04 wt.%, respectively).

Olivine II forms anhedral, scarcely subhedral crystals varying in size from 10 to 250 μm. Despite variable textural positions of the olivine II (crystals in aggregate, crystals enveloping orthopyroxene I, crystals in decomposed orthopyroxene) its composition show the same relations to composition of olivine I. The Fo content in olivine II is usually close to that in olivine I in given xenolith; only in subhedral crystals the Fo is lower ($Fo_{86.65}$ in group A and $Fo_{84.78}$ in group B; Figure 5, Table 4).

The Ol II is always depleted in NiO (0.396–0.186 wt.%) and dramatically enriched in Ca (800–2665 ppm) compared to Ol I; the highest contents of Ca occur in rims of crystals.

Vermicular to angular crystals of clinopyroxene II from first to 20 μm wide envelope some of the orthopyroxene I crystals; if they are developed to mixture with olivine II and glass, the whole structure is oval with the longer axis of ca. 400 μm. This

Table 3. Representative analyses of glass

No.	1	2	3	4	5	6	7	8	9	10	11	12
Textural position	DOpx	DOpx	Opx assoc	Opx assoc	Opx assoc	Opx assoc	Opx assoc	A	A	A	A	A
SiO_2	67.695	67.496	58.854	58.977	67.077	67.274	61.223	63.667	67.194	64.621	58.695	59.640
TiO_2	0.037	0.028	1.074	1.075	0.391	0.301	1.524	1.093	0.044	0.293	1.032	0.914
Al_2O_3	16.511	15.817	22.502	22.498	18.495	18.160	22.056	19.798	17.190	19.099	23.508	23.822
Cr_2O_3	0.024	0.023	0.012	0.002	0.020	0.040	0.012	0.022	0.053	0.085	0.027	0.020
FeO*	0.993	1.145	0.961	0.997	0.411	0.509	1.036	0.417	0.838	0.704	1.114	0.876
MnO	0.038	0.000	0.019	0.022	0.000	0.018	0.028	0.003	0.013	0.030	0.021	0.000
NiO	0.001	0.011	0.029	0.000	0.026	0.000	0.000	0.035	0.001	0.000	0.010	0.000
MgO	0.840	2.648	0.421	0.345	0.131	0.148	0.532	0.343	0.662	0.712	0.668	0.387
CaO	0.070	0.052	0.405	0.541	0.167	0.176	0.202	0.751	0.049	0.101	0.570	0.584
Na_2O	3.918	3.805	4.041	4.281	7.490	7.090	3.498	7.464	3.456	3.376	4.093	4.091
K_2O	5.819	5.393	6.209	6.188	6.183	6.686	5.062	5.268	4.989	5.946	5.917	5.077
Total	95.946	96.418	94.527	94.926	100.441	100.419	95.173	98.861	94.489	94.967	95.655	95.411
NaO+K2O	9.737	9.198	10.250	10.469	13.673	13.776	8.560	12.732	8.445	9.322	10.010	9.168
mg#	0.602	0.805	0.439	0.382	0.363	0.342	0.478	0.595	0.585	0.644	0.517	0.441

* — total iron; DOpx — glass in decomposing Opx I; Opx assoc — glass in reaction zones around Opx I; A — glass in aggregates.

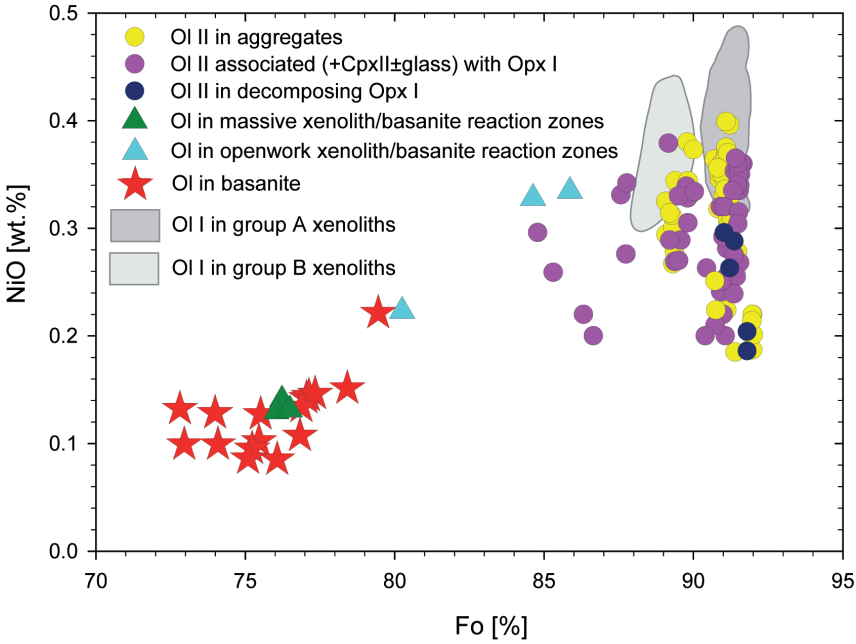

Figure 5. Fo-NiO relationships in olivine II from Krzeniów xenoliths and xenolith/basanite reaction zones compared to olivine I. Data for olivine I after (Matusiak-Małek 2010)

clinopyroxene II has composition of ± Ti, Cr diopside/augite. Compared to clinopyroxene I, clinopyroxene II associated with orthopyroxene I is depleted in Al and Ca and enriched in Ti, while content of other elements is similar (Figure 6, Table 4).

Clinopyroxene II which is not associated with orthopyroxene I forms sub- to anhedral crystals up to 300 μm in size, typically 10–90 μm. Their cores are massive or patchy, the rims are spongy (Figure 2g). Spongy clinopyroxene II often encloses minute inclusions of glass or feldspar. Composition of clinopyroxene II depends on its texture. Some parts (especially cores) of patchy crystals have composition identical or similar to clinopyroxene I in a given xenolith; in outer parts clinopyroxene II has a composition of ± Ti, ± Al, Cr-diopside/augite and displays lower mg-numbers (down to 0.82), Si and Ca contents, while Al, Ti and Cr are higher (Figure 6, Table 5). The same relationships are true for massive clinopyroxene II with spongy rims, where massive parts have composition identical to clinopyroxene I.

Parts of clinopyroxene I grains contacting with plagioclase-bearing aggregate have composition of Al, Cr-diopside (mg# = 0.915–0.924). Compared to clinopyroxene I, it is enriched in Al and Cr, while contents of Na and Si are lower (Figure 6, Table 5).

Only few successful analyses of clinopyroxene II occurring in decomposed orthopyroxene I were made due to its small size. It has composition of Al-diopside depleted in Al and Ca in comparison to clinopyroxene I (Figure 6; Table 5).

Table 4. Representative analyses and structural formulae (O^{2-} = 4) of olivine II

No.	1	2	3	4	5	6	7	8	9	10	11	12	13
Textural position	DOpx	DOpx	Opx assoc	Opx assoc	A	A	A	E	E	MR	MR	OR	OR
Group of primary grains	B	B	A	A	A	A	A	A	B	A	A	B	B
SiO_2	41.095	41.504	40.374	41.210	39.651	40.297	40.227	41.710	37.988	38.500	38.290	39.182	40.026
TiO_2	0.030	0.010	0.000	0.011	0.022	0.026	0.010	0.000	0.049	—	—	0.003	0.01
Al_2O_3	0.092	0.028	0.009	0.018	0.023	0.171	0.026	—	0.038	0.030	0.020	0.005	0.003
Cr_2O_3	0.081	0.071	0.020	0.085	0.141	0.068	0.111	0.030	0.036	0.040	0.030	0.025	0.029
FeO*	8.721	8.563	9.886	8.314	9.087	10.403	7.928	8.850	14.370	21.810	21.520	18.459	13.633
MnO	0.128	0.171	0.142	0.142	0.187	0.239	0.157	0.210	0.276	0.480	0.480	0.399	0.279
NiO	0.296	0.263	0.328	0.365	0.364	0.294	0.201	0.200	0.296	0.130	0.130	0.223	0.335
MgO	49.629	49.895	48.860	49.665	49.701	47.656	51.181	50.590	44.917	38.870	39.090	42	46.463
CaO	0.110	0.189	0.272	0.179	0.301	0.295	0.141	0.180	0.373	0.460	0.460	0.323	0.165
Na_2O	0.009	0.029	0.020	0.004	0.007	0.010	0.020	—	0.050	—	—	0.006	0.008
K_2O	0.000	0.005	0.001	0.001	0.000	0.000	0.031	—	0.010	—	—	0.003	0.002
Total	100.191	100.728	99.912	99.994	99.484	99.459	100.033	101.770	98.403	100.320	100.020	100.628	100.953
Si^{+4}	1.001	1.004	0.993	1.004	0.979	0.998	0.981	1.000	0.974	0.998	0.995	0.996	0.992
Ti^{+4}	0.001	0.000	0.000	0.000	0.000	0.000	0.000	0.000	0.001	—	—	0.000	0.000
Al^{+3}	0.003	0.001	0.000	0.001	0.001	0.005	0.001	0.000	0.001	0.001	0.001	0.000	0.000
Cr^{+3}	0.002	0.001	0.000	0.002	0.003	0.001	0.002	0.001	0.001	0.001	0.001	0.001	0.001
Fe^{+2}	0.178	0.173	0.203	0.169	0.188	0.215	0.162	0.178	0.308	0.473	0.468	0.392	0.282
Mn^{+2}	0.003	0.004	0.003	0.003	0.004	0.005	0.003	0.004	0.006	0.011	0.011	0.009	0.006
Ni^{+2}	0.006	0.005	0.006	0.007	0.007	0.006	0.004	0.004	0.006	0.003	0.003	0.005	0.007
Mg^{+2}	1.802	1.800	1.792	1.804	1.829	1.759	1.860	1.809	1.716	1.502	1.514	1.592	1.716
Ca^{+2}	0.003	0.005	0.007	0.005	0.008	0.008	0.004	0.005	0.010	0.013	0.013	0.009	0.004
Na^{+1}	0.000	0.001	0.001	0.000	0.000	0.000	0.001	0.000	0.002	—	—	0.000	0.000
K^{+1}	0.000	0.000	0.000	0.000	0.000	0.000	0.001	—	0.000	—	—	0.000	0.000
Total	2.997	2.995	3.007	2.995	3.019	2.999	3.019	3.000	3.026	3.001	3.004	3.004	3.008
Fo [%]	91.0	91.2	89.8	91.4	90.7	89.0	92.0	91.1	84.8	76.0	76.4	80.2	85.9
Ca [ppm]	786	1351	1944	128	2151	2108	1008	1286	2666	3288	3288	2308	1179

* — total iron; DOpx — Ol II in decomposing Opx I; Opx assoc — Ol II in reaction zones around Opx I; A — Ol II in aggregates; E — euhedral grains of Ol II; MR — Ol in massive xenolith/basanite reaction zones; OR — Ol in openwork xenolith/basanite reaction zones.

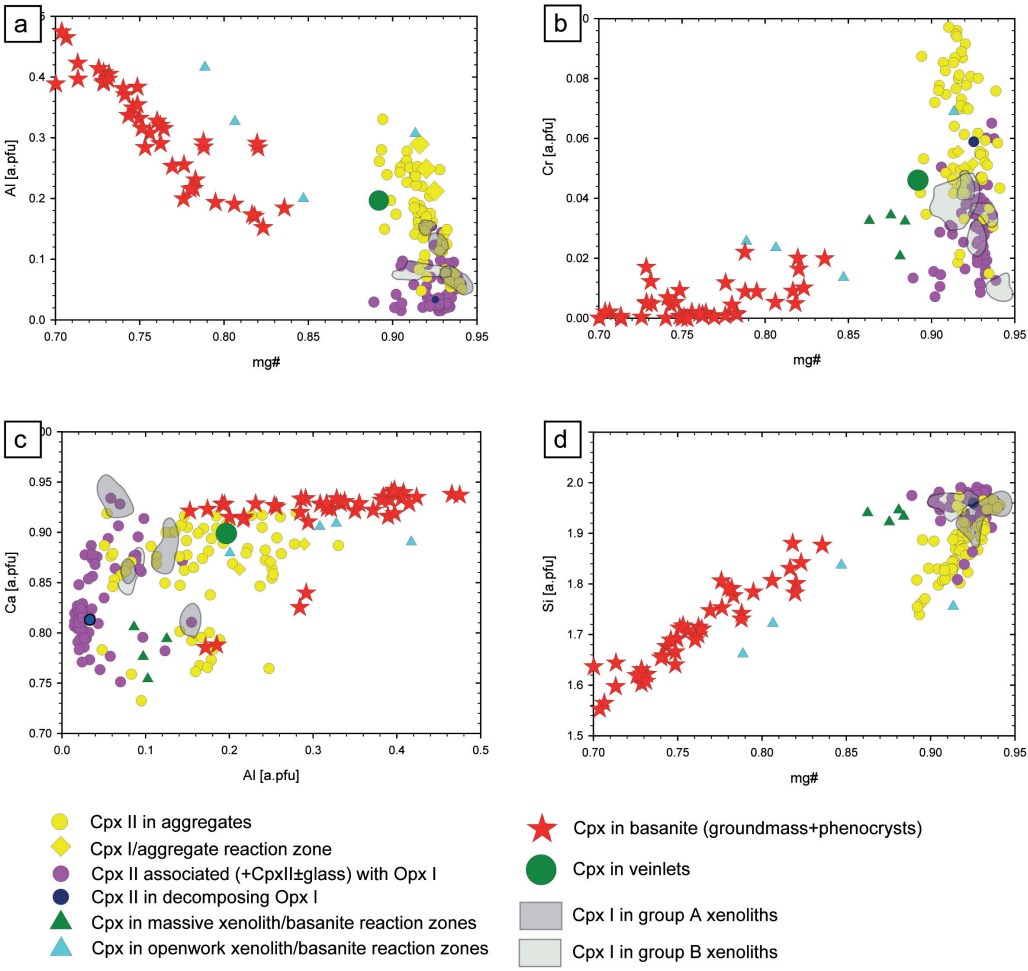

Figure 6. Composition of clinopyroxene II compared to composition of clinopyroxene I and clinopyroxene from host basanite. (a) mg# vs. Al, (b) mg# vs. Cr, (c) Al vs. Ca, (d) mg# vs.Si. Data for clinopyroxene I after (Matusiak-Małek 2010)

Spinel II forms massive (with fringed rims) and skeletal crystals varying in size from few to ca. 40 µm. Despite cr- and mg-numbers (0.317–0.766 and 0.338–0.761, respectively) are only negligibly different from those in primary spinel in a given xenolith, TiO_2 content is variable in significantly wider ranges (0.02 to 6.43 wt.% in spinel II vs. up to 0.973 wt.% in spinel I, Table 6). In some of the aggregates, larger (up to 1.5 mm) crystals of spinel with fringe margins occur. Their chemical composition is the same as that of spinel I with almost negligible enrichment in Ti content in the rims. Spinel occurring in veinlet has variable composition of mg# = 0.410–0.598 and cr#= 0.353–0.635.

Apatite occurs scarcely in veinlets as elongated (20–45 µm), subhedral crystals from first to 20 µm in diameter (Figure 2b). It has a composition of fluorapatite with F content varying from 2.29 to 3.16 wt.%; some grains are also Cl-rich (up to 1.09 wt.%).

Table 5. Representative analyses and structural formulae (O^{2-} = 6) of clinopyroxene II

No.	1	2	3	4	5	6	7	8	9	10	11	12	13	14	15	16
Textural position	Opx assoc	Opx assoc	Opx assoc	Opx assoc	A	A	A	A	DOpx	DOpx	RA	RA	MR	MR	OR	OR
Group of primary grains	A	A	B	B	A	A	B	B	B	A	B	B	A	A	B	B
SiO_2	53.980	52.635	52.308	54.075	53.485	46.923	49.099	53.629	48.753	53.270	47.574	43.975	53.110	52.910	47.574	43.975
TiO_2	0.025	0.064	1.100	0.126	0.007	0.103	0.297	0.177	2.989	0.012	1.762	3.886	0.390	0.400	1.762	3.886
Al_2O_3	1.372	3.593	2.120	2.083	1.248	7.466	4.474	1.184	4.496	0.769	7.119	9.440	2.390	1.990	7.119	9.440
Cr_2O_3	0.351	1.519	1.460	1.004	0.513	2.943	3.444	1.504	1.570	2.024	2.384	0.873	1.130	1.130	2.384	0.873
FeO*	1.997	2.485	2.592	3.159	2.201	3.142	3.035	1.968	3.221	2.628	2.478	5.658	4.260	4.810	2.478	5.658
MnO	0.095	0.076	0.061	0.098	0.086	0.031	0.067	0.074	0.076	0.099	0.079	0.142	0.170	0.210	0.079	0.142
NiO	0.066	0.070	0.074	0.042	0.050	0.080	0.047	0.032	0.052	0.052	0.027	0.054	0.010	0.020	0.027	0.054
MgO	17.796	16.752	16.929	16.882	17.627	14.889	15.126	17.628	14.903	18.288	14.669	11.845	18.230	16.950	14.669	11.845
CaO	24.082	20.690	22.919	22.673	23.396	22.051	22.731	22.697	22.624	20.623	23.041	22.174	19.340	20.510	23.041	22.174
Na_2O	0.256	1.300	0.731	0.723	0.640	0.643	0.733	0.772	0.767	1.088	0.546	0.830	0.740	0.760	0.546	0.830
K_2O	0.000	0.015	0.006	0.000	0.016	0.000	0.060	0.055	0.011	0.041	0.000	0.011	—	—	0.000	0.011
Total	100.020	99.199	100.300	100.865	99.269	98.271	99.113	99.720	99.462	98.894	99.679	98.888	99.770	99.690	99.679	98.888
Si^{+4}	1.954	1.924	1.907	1.953	1.960	1.761	1.831	1.956	1.808	1.960	1.747	1.649	1.935	1.942	1.757	1.663
Ti^{+4}	0.001	0.002	0.030	0.003	0.000	0.003	0.008	0.005	0.083	0.000	0.049	0.110	0.011	0.011	0.049	0.111
Al^{+3}	0.059	0.155	0.091	0.089	0.054	0.330	0.197	0.051	0.196	0.033	0.308	0.417	0.103	0.086	0.310	0.421
Cr^{+3}	0.010	0.044	0.042	0.029	0.015	0.087	0.102	0.043	0.046	0.059	0.069	0.026	0.033	0.033	0.070	0.026
Fe^{+2}	0.060	0.076	0.079	0.095	0.067	0.099	0.095	0.060	0.100	0.081	0.076	0.177	0.130	0.148	0.077	0.179
Mn^{+2}	0.003	0.002	0.002	0.003	0.003	0.001	0.002	0.002	0.002	0.003	0.002	0.005	0.005	0.007	0.002	0.005
Ni^{+2}	0.002	0.002	0.002	0.001	0.001	0.002	0.001	0.001	0.002	0.002	0.001	0.002	0.000	0.001	0.001	0.002
Mg^{+2}	0.960	0.913	0.920	0.909	0.963	0.833	0.841	0.958	0.824	1.003	0.803	0.662	0.990	0.927	0.808	0.668
Ca^{+2}	0.934	0.810	0.895	0.877	0.919	0.887	0.908	0.887	0.899	0.813	0.906	0.891	0.755	0.807	0.912	0.899
Na^{+1}	0.018	0.092	0.052	0.051	0.045	0.047	0.053	0.055	0.055	0.078	0.039	0.060	0.052	0.054	0.039	0.061
K^{+1}	0.000	0.001	0.000	0.000	0.001	0.000	0.003	0.003	0.001	0.002	0.000	0.001	—	—	0.000	0.001
Total	4.000	4.021	4.022	4.010	4.028	4.050	4.040	4.021	4.016	4.033	4.000	4.000	4.013	4.015	4.024	4.034
mg#	0.941	0.923	0.921	0.905	0.935	0.894	0.899	0.941	0.892	0.925	0.913	0.789	0.884	0.863	0.913	0.789

* — total iron; Opx assoc — Ol II in reaction zones around Opx I; A — Ol II in aggregates; DOpx — Ol II in decomposing Opx I; RA — Cpx I reacting with aggregate; MR — Ol in massive xenolith/basanite reaction zones; OR — Ol in openwork xenolith/basanite reaction zones.

Table 6. Representative analyses and structural formulae (K = 3) of spinel II

No.	1	2	3	4	5	6	7	8	9	10	11	12	13
Textural position	Spl II	Spl II	Spl II	Spl II	Spl II	Spl A	Spl A	Spl A	Spl A	Spl A	MR	MR	OR
Group of primary grains	A	A	A	B	B	A	A	A	A	A	A	A	B
SiO_2	0.081	0.013	0.066	0.023	0.057	0.021	0.000	0.014	0.019	0.04	0.050	0.050	0.06
TiO_2	0.868	0.018	0.088	3.847	5.182	0.114	0.227	0.239	0.012	0.97	20.980	21.690	2.09
Al_2O_3	38.376	21.666	38.069	9.532	21.399	32.227	9.371	9.429	15.186	19.66	5.580	6.000	25.36
Cr_2O_3	26.603	47.259	30.293	46.402	30.728	34.724	54.790	54.632	52.146	45.75	2.640	2.590	29.56
FeO*	14.981	14.665	10.308	23.848	29.891	14.017	21.086	21.096	17.585	18.11	61.580	60.530	26.70
MnO	0.115	0.110	0.111	0.310	0.410	0.156	0.215	0.211	0.198	0.15	0.670	0.680	0.30
NiO	0.231	0.140	0.136	0.111	0.216	0.173	0.161	0.150	0.108	0.14	0.090	0.070	0.27
MgO	16.873	14.945	18.362	10.848	9.606	16.607	12.472	12.353	13.299	13.44	3.970	4.480	12.75
CaO	0.077	0.016	0.044	0.067	0.077	0.041	0.000	0.000	0.055	0.11	0.260	0.100	0.07
Na_2O	0.017	0.002	0.035	0.000	0.017	0.000	0.000	0.000	0.017	0.01	0.010	0.000	0.00
K_2O	0.000	0.010	0.001	0.048	0.035	0.000	0.004	0.000	0.000	0.01	—	—	0.01
Total	98.141	98.831	97.447	95.036	97.618	98.080	98.326	98.124	98.625	98.34	95.830	96.190	97.16
Si^{+4}	0.002	0.000	0.002	0.001	0.002	0.001	0.000	0.000	0.001	0.00	0.002	0.002	0.00
Ti^{+4}	0.019	0.000	0.002	0.099	0.125	0.003	0.006	0.006	0.000	0.02	0.571	0.586	0.05
Al^{+3}	1.291	0.784	1.279	0.385	0.809	1.113	0.364	0.367	0.571	0.73	0.238	0.254	0.93
Cr^{+3}	0.601	1.147	0.683	1.259	0.780	0.805	1.427	1.426	1.315	1.13	0.076	0.074	0.72
Fe^{+3}	0.067	0.068	0.033	0.158	0.159	0.075	0.198	0.194	0.113	0.09	0.541	0.497	0.25
Fe^{+2}	0.290	0.309	0.213	0.526	0.643	0.268	0.383	0.388	0.356	0.38	1.324	1.321	0.44
Mn^{+2}	0.003	0.003	0.003	0.009	0.011	0.004	0.006	0.006	0.005	0.00	0.021	0.021	0.01
Ni^{+2}	0.005	0.003	0.003	0.003	0.006	0.004	0.004	0.004	0.003	0.00	0.003	0.002	0.01
Mg^{+2}	0.718	0.684	0.780	0.555	0.460	0.726	0.612	0.608	0.633	0.63	0.214	0.240	0.59
Ca^{+2}	0.002	0.001	0.001	0.002	0.003	0.001	0.000	0.000	0.002	0.00	0.010	0.004	0.00
Na^{+1}	0.001	0.000	0.002	0.000	0.001	0.000	0.000	0.000	0.001	0.00	0.001	0.000	0.00
K^{+1}	—	0.000	0.000	0.002	0.001	0.000	0.000	0.000	0.000	0.00	—	—	0.00
Total	3.000	3.000	3.000	3.000	3.000	3.000	3.000	3.000	3.000	3.00	3.000	3.000	3.00
mg#	0.668	0.645	0.761	0.448	0.364	0.730	0.513	0.511	0.640	0.57	0.103	0.117	0.46
cr#	0.317	0.594	0.348	0.766	0.491	0.420	0.797	0.795	0.697	0.61	0.241	0.225	0.44

* — total iron; Spl A — Spl I in aggregate; MR — massive xenolith/basanite reaction zone; MR — openwork xenolith/basanite reaction zone.

Sulfides form anhedral, oval (50–400 μm long, Figure 2h) grains consisting of cores of Ni-pyrrhotite with pentlandite intergrowths, surrounded by pentlandite rims. Also smaller (20–50 μm) intergranular crystals of pure pentlandite and chalcopyrite occur (Table 7).

Table 7. Representative analyses of sulfides

No.	1	2	3	4	5	6	7
Textural position	R	R	C	C	H	H	H
Mineral	Pn	Pn	Ni-Po	Ni-Po	Pn	Pn	Pn
Si	0.023	0.017	0.016	0.016	0.050	0.030	0.015
S	33.512	33.534	39.431	39.595	33.505	32.999	33.384
Fe	29.279	29.288	54.574	56.886	30.257	30.407	30.429
Co	0.566	0.593	0.006	0.015	0.511	0.491	0.447
Ni	33.688	34.106	3.850	1.306	33.736	33.616	33.779
Total	97.068	97.537	97.876	97.818	98.059	97.543	98.053

R— rim, C — core, H — homogeneous

4.1.3. Contact with basanite

Three types of basanite/xenolith contact occur in Krzeniów xenoliths: (1) sharp, (2) massive reaction zone and (3) openwork reaction zone (Figure 7). Openwork and massive reaction zones never occur along the same xenolith, but sharp contact may coexist with any of the type of reaction zones.

Massive reaction zone is the dominating type of basanite/xenolith reaction. The massive zone is formed either by large subhedral crystals of clinopyroxene or mixture of sub- to anhedral clinopyroxene, orthopyroxene, spinel and apatite embedded in olivine matrix (Figure 7a). Width of the reaction zones is from first μm to 20 μm if formed by clinopyroxene crystals and up to 300 μm if formed of mixture of crystals. The olivine ($Fo_{76.06-76.40}$) is rich in Ca (3200–3300 ppm) and relatively poor in NiO (0.13–0.14 wt.%, Table 4). The clinopyroxene in the mixtures is rounded and has composition of ± Al, Cr-diopside/augite (mg# = 0.863–0.884; Table 5). Orthopyroxene forms 300 μm long anhedral crystals with lobate borders; it has the composition of ± Cr enstatite (#mg = 0.917–0.919) and it is probably a remnant of not-fully reacted orthopyroxene I. Spinel is massive and subhedral and has composition of ülvospinel (#mg = 0.103–0.117, #cr = 0.225–0.241, Table 6). Apatite forms scarce subhedral crystals up to 30μm in cross section and contains elevated amounts of F, but no quantitative data are available.

The "openwork" reaction zone is formed of angular, 1 cm x 600 μm rectangular (in cross section) zones unequally distributed at the xenolith/basanite border. The "rectangles" are formed of clinopyroxene, plagioclase and opaques. The clinopyroxene forms narrow (up to 30 μm) elongated (from first to 400 μm) crystals parallel or perpendicular (in single "rectangle") to the xenolith margin (Figure 7b,c). At the xenolith/"rectangle" contact subhedral, angular crystals of

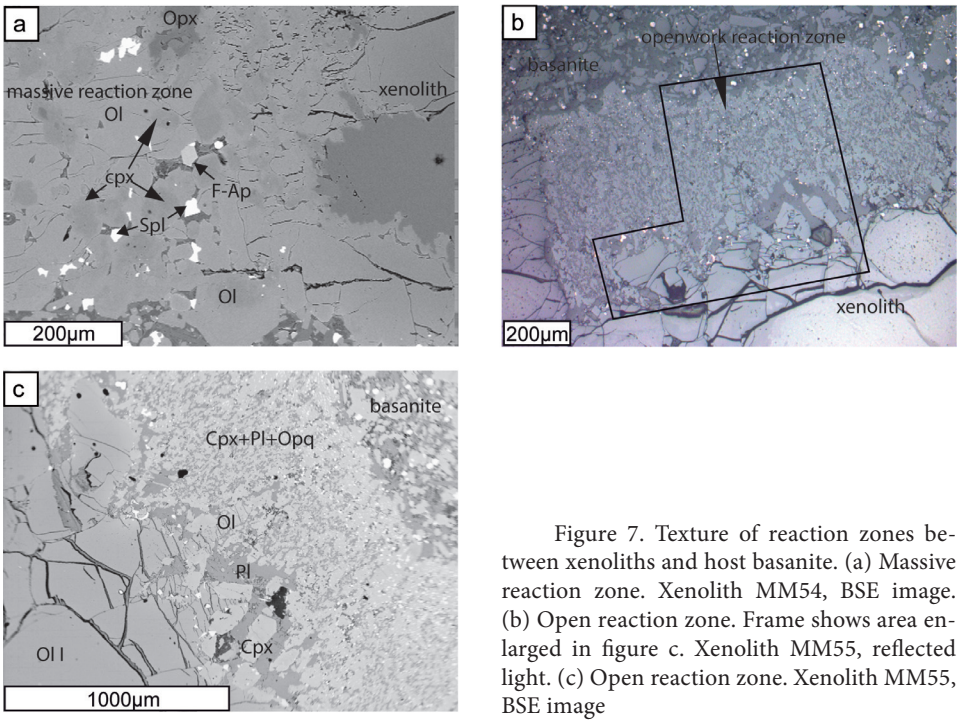

Figure 7. Texture of reaction zones between xenoliths and host basanite. (a) Massive reaction zone. Xenolith MM54, BSE image. (b) Open reaction zone. Frame shows area enlarged in figure c. Xenolith MM55, reflected light. (c) Open reaction zone. Xenolith MM55, BSE image

clinopyroxene and laths of feldspar ± olivine occur. The clinopyroxene occurring in rectangular zones has composition of Ti, Al, Cr-diopside and strongly variable mg-number (0.789–0.847); the subhedral crystals have similar composition, but their mg# is 0.913. Olivine is strongly heterogeneous, the Fo content decreases from 85.87 in proximity to the xenolith to 80.22 in distance from the xenolith; the Fo is negatively correlated with Ca (2300–1180 ppm) and NiO (0.223–0.335 wt.%) contents. Plagioclase has composition of $An_{54-55}Or_2Ab_{42-43}$, while mg# and cr# in spinel are 0.46 and 0.44, respectively.

5. Origin of the aggregates

The aggregates occur in various textural positions in the xenoliths. Those forming the intergranular "patches" could have originated due to melt infiltration or breakdown of hydrous phases, whereas those rimming orthopyroxene are due to its reaction with a melt. The apatite-bearing veinlets continue from host basanite and possibly originated due to its infiltration into the xenoliths.

Clinopyroxene occurring at clinopyroxene I/aggregate contact is enriched, compared to clinopyroxene I, in Al and Cr, while Si, Na, Ca and mg# are diminished. The same relations occur between clinopyroxene II from aggregates and

primary clinopyroxene in all the xenoliths. Moreover, composition of cores of some of the aggregate clinopyroxene II mimics composition of clinopyroxene I in given xenolith. Thus, clinopyroxene II in aggregates is not a newly crystalized phase, but was formed due to reaction of clinopyroxene I with a melt. The same is true for spinel II occurring in aggregates — cores of larger grains almost perfectly mimic composition of spinel I, while outer parts and small crystals differ from spinel I only in higher Ti content. Also olivine II in the aggregates follows chemical features of olivine I in given xenolith except of Ca content which is strongly elevated, especially in the rims. Remnants of primary phases in secondary clinopyroxene, olivine and spinel show that intergranular aggregates were formed due to reaction with infiltrating melt. As the aggregate minerals display strong chemical heterogeneity, we assume that the melt-xenolith reaction must have been very short.

The composition of the infiltrating melt is potentially recorded by trachyandesite/trachydacite glass occurring in aggregates (Figure 4). However, the composition of glasses varies in wide ranges suggesting either multiple infiltrations by melts of at least four different compositions or blur of the primary composition by further processes (mixing, reaction with peridotite minerals, devitrification, etc). Moreover, it is impossible to distinguish truly infiltrating melts from that produced by reaction between infiltrating agents and host minerals. Thus, we do not use composition of glasses as referential composition of infiltrating melt.

Composition of the infiltrating melt may be estimated only on a base of effects it caused during reaction with peridotite minerals or on composition of newly formed phases. Presence of sulfides (Ni-pyrrhotite, pentlandite, chalcopyrite) in some of the fine-grained aggregates in the Krzeniów xenoliths suggests that the infiltrating silicate melt was relatively sulphur rich contained; in some of the crystalizing aggregates it reached sulfide saturation during crystallization. Olivine in aggregates do not record any significant changes in Fo content which stands for mafic/ultramafic nature of the melt. Thus, the possible medium leading to fine-grained aggregates formation was a Si-undersaturated S-bearing silicate melt.

The aggregates always contain clinopyroxene II, which is present even in clinopyroxene I-free xenoliths. Possible origins of clinopyroxene II in such xenoliths are: (1) reaction of clinopyroxene I with the melt, (2) clinopyroxene II formation due to melt/orthopyroxene I reaction and (3) crystallization of clinopyroxene from the infiltrating melt. Possibility (1) is evident in xenolith where crystals of clinopyroxene II preserve the crystallographic orientation of replaced clinopyroxene I (Figure 2f). In this xenolith reaction of clinopyroxene I with melt was frozen at very early stage and before the newly formed grains were reoriented and fully chemically reequilibrated. Similar process but with random reorientation of clinopyroxene II crystals was possible also in other xenoliths. Possibility (2) is support-

ed by composition of clinopyroxene II from aggregates, which partly overlaps with composition of clinopyroxene II associated with orthopyroxene I. No textural evidence supports scenario (3) and thus it seems to be the least possible.

Breakdown of hydrous phases (amphibole and phlogopite) may be also responsible for formation of intergranular aggregates (Aliani et al. 2009; Shaw 2009). Amphibole breakdown leads to formation of secondary olivine, clinopyroxene, spinel and melt/glass, while olivine, enstatite and melt/glass are possible products of phlogopite melting (Yoder and Kushiro 1969). As secondary enstatite does not occur in intergranular aggregates, breakdown of phlogopite could not have been responsible for aggregates formation.

The Krzeniów xenolith suite is modally anhydrous. It however may be assumed that all the hypothetical amphibole had been decomposed. To test this hypothesis we have estimated the composition of hypothetical amphibole with use of least-square method presented by Aliani et al. (2009). Comparison with composition of pargasitic amphibole from Wilcza Góra xenoliths (the closest xenolith-bearing locality od volcanic rock; Matusiak-Małek 2010) gave $\Sigma r^2 >> 1$ which corresponds to lack of similarities in chemical composition between the hypothetical and natural amphibole. Thus we conclude that the formation of intergranular aggregates was not related to breakdown of any hydrous phase.

Orthopyroxene I contacting with aggregates is always rimmed by mixture of clinopyroxene II ± olivine II ± glass; occasionally, the rims occur also in orthopyroxene I beyond the aggregates. Such structures are described in mantle xenoliths worldwide (e.g. Dawson 2002; Yaxley et al. 1997). Close association of the rim with orthopyroxene I clearly suggest that formation of this type of clinopyroxene II is related to orthopyroxene I dissolution. This hypothesis is further supported by image (Figure 2e) of frozen process of dissolution of orthopyroxene I to olivine II, clinopyroxene II and glass. Shaw (1999) and Shaw et al. (1998) have experimentally examined the process of orthopyroxene dissolution in silica undersaturated melt. The experiments show that under pressure exceeding 1 GPa orthopyroxene reacting with Si-poor solvent dissolves to olivine, glass and clinopyroxene. The dissolution reaction is two-step: (1) orthopyroxene reacts with the melt dissolving incongruently and forming forsterite and glass reaction zone; (2) Ca and Al from the solvent diffuse inward the reaction zone (towards orthopyroxene) causing saturation in clinopyroxene, while Si diffuses in the opposite direction. This model seems to fit texturally to the image recorded in Krzeniów xenoliths. As the rims occur around orthopyroxene I contacting with aggregates but also around grains beyond the structures, the solvent must have percolated along primary grains of peridotite. The reaction was fast in majority of the xenoliths as composition of clinopyroxene II may vary significantly even in scale of few tens of μm.

The plagioclase-apatite veinlets contain plagioclase having similar core composition as basanitic plagioclase (Figure 3; Matusiak-Małek 2010). Composition of spinel occurring in veinlets is typical for magmatic spinel enclosed in magmatic

olivine in undersaturated lavas. Large crystals of fluorapatite present in veinlets in significant amounts were not reported from the Krzeniów basanite where apatite grains are acicular and rather discrete (Białowolska 1993; Birkenmajer et al. 2007; Ladenberger 2006; Matusiak-Małek 2010). On the other hand, apatite is present in massive xenolith/basanite reaction zones, thus it might have been formed due to reaction with the same melt whose infiltration led to veinlets formation. Large (up to 7 mm long) apatite crystals were described from diopside megacrysts from Ostrzyca basanite located 13 km SW from Krzeniów (D. Lipa unpublished data). The megacrysts are interpreted to come from disintegrated cumulate formed at uppermost mantle/lower crust depths by crystallization from primary alkaline silicate melt. A similar melt may have intruded into Krzeniów xenoliths and form massive reaction zones, but relations between the phosphorous-bearing melt and Krzeniów basanite are unknown.

The composition of clinopyroxene and plagioclase forming the openwork xenolith/basanite reaction zone mimic those of the phases in basanite, while olivine in the reaction zones is depleted in Fo and NiO and enriched in Ca. As Fo contents in majority of olivine II crystals is not diminished in comparison to that in olivine I, formation of intergranular aggregates due to reaction with host basanite is not possible.

6. Conclusions

The chemical characteristic of Krzeniów mantle rocks (harzburgites, dunites) was established by melting and metasomatic events of probably Variscan age. The fine-grained aggregates occurring in xenoliths from the Krzeniów basanite are much younger and record infiltration/percolation of the S-bearing, silica-undersaturated alkali silicate melt. The aggregates in all the types of xenoliths display similar composition and structure, therefore they probably come from one mantle section or originated after the separation of xenoliths from host mantle sequences and their entrainment into the basanite magma. Thus, the S-bearing melt could not have been related to any of the metasomatic agents proposed for Krzeniów mantle (Si-undersaturated, CO_2-rich alkaline and Fe-rich melts; Matusiak-Małek 2010). However, infiltration of the melt and reaction with peridotite phases has to be considered as metasomatic events: changes in chemical composition of clinopyroxene, orthopyroxene and spinel fulfil condition of cryptic metasomatism, while crystallization of sulfides and feldspar is an example of modal metasomatism. Presence of aggregates formed by mafic melts infiltrating peridotite prior to magma entrapment was documented also for other mantle xenoliths in Lower Silesia: Księginki (Puziewicz et al. 2011) and Lutynia (Matusiak-Małek et al. 2010), however Krzeniów is the only locality, where the melt was S-bearing.

Composition of glass occurring in reaction zones around orthopyroxene I zones varies from trachyandesite to trachydacite/dacite partly overlapping the composition of glass occurring in aggregates. This suggests that both aggregates and zones around orthopyroxene I may be related to reaction with the same melt.

The next episode in the Krzeniów peridotite history took place after formation of xenolith, i.e. at crustal levels. In the crust the fissures in xenoliths were infiltrated by P-rich melt which crystallized into plagioclase + apatite mineral assemblage. The very last episode recorded in the xenoliths is a formation of basanite/xenoliths reactions zones. The zones are either thin or completely missing but their presence required stagnation in magma chamber (Klügel 1998). Lack of detailed chemical profiles in minerals forming reaction zones did not allow us to calculate the time of residence in magma chamber.

The late stage process recorded in aggregates, veinlets and reaction zones around xenoliths may blur or obscure the general image of upper mantle recorded in host peridotite. At the same time they evidence short events preceding entrapment by ascending magma.

Acknowledgements

We are very grateful to the management of "Przedsiębiorstwo Górniczo-Produkcyjne BAZALT S.A." in Wilków for support during field works. We thank Dr Antoni Muszer for consultations regarding the sulfide minerals. The analytical work was possible thanks to the "Iuventus Plus" project funded by the Polish Ministry of Science and Higher Education to MMM.

References

Albrycht A., J. Badura, A. Ber, M. Jastrzębska-Ber, M. Bruj, M. Brzeziński, R. Chmal, Z. Cymerman, E. Dobracka, R. Dobracki, A. Frankiewicz, D. Gałązka, J. Haising, E. Jeleńska, L. Jurys, A. Krajewska, M. Krawczyk, Z. Krysiak, T. Krzywicki, M. Lichwa, S. Lisicki, S. Marszałek, W. Morawski, D. Nizicka, R. Pikies, K. Piotrowska, A. Piotrowski, K. Pochocka-Szwarc, W. Prussak, J. Przasnyska, B. Przybylski, A. Romanek, J. Rumiński, J. Rychel, H. Szalewicz, A. Ślesińska, R. Wasiluk, A. Wełniak, S. Wilanowski, J. Winnicki, A. Wójcik, R. Zabielski, L. Zaleszkiewicz, Z. Zimnal, M. Żarski. 2006. *Mapa geologiczna Polski 1:500 000*. L. Marks, A. Ber, W. Gogołek, K. Piotrowska (eds.). Warszawa.

Aliani P., T. Ntaflos, E. Bjerg. 2009. Origin of melt pockets in mantle xenoliths from southern Patagonia, Argentina. *Journal of South American Earth Sciences*, 28, pp. 419–428.

Bakun-Czubarow N., A. Białowolska. 2003. Gabbroic enclaves from basaltoids of the Lubań and Złotoryja regions, Lower Silesia. *Xth meeting of the Petrology Group of the Mineralogical Society of Poland*, 23, pp. 32–34.

Bakun-Czubarow N., A. Białowolska. 2005. Internal blebs within mantle peridotite enclaves from Lower Silesia basaltoids-preliminary results. *The 12th meeting of the Petrology Group of the Mineralogical Society of Poland*, 26, pp. 124–129.

Białowolska A. 1993. Enklawy w bazaltoidach wzgórz Łysanka i Trupień (Dolny Śląsk). *Archiwum Mineralogiczne*, 49, pp. 145–197.

Birkenmajer K., J. Jerzmański, A.E.M. Nairn, Paleomagnetic studies of Polish rocks. IV. Cenozoic basalts of Lower Silesia. *Annales Societatis Geologorum Poloniae*, XL, pp. 31–61.

Birkenmajer K., M.W. Lorenc, Z. Pécskay, P.P. Zagożdżon. 2004a. Wiek, cykle i kierunek migracji trzeciorzędowego bazaltowego wulkanizmu Dolnego Śląska w świetle datowań K–Ar. *VIII Ogólnopolska Konferencja Naukowa „Datowanie minerałów i skał"*, pp. 9–10.

Birkenmajer K., Z. Pécskay. 2002. Radiometric dating of the Tertiary volcanics in Lower Silesia, Poland. I. Alkali basaltic rocks of the Opole region. *Bulletin of the Polish Academy of Sciences. Earth Sciences*, 50, pp. 31–50.

Birkenmajer K., Z. Pécskay, J. Grabowski, M.W. Lorenc, P.P. Zagożdżon. 2002. Radiometric dating of the Tertiary volcanics in Lower Silesia, Poland. III. K-Ar and paleomagnetic data from early Miocene basaltic rocks near Jawor, Fore–Sudetic Block. *Annales Societatis Geologorum Poloniae*, 72, pp. 241–253.

Birkenmajer K., Z. Pécskay, J. Grabowski, M.W. Lorenc, P. Zagożdżon. 2004b. Radiometric dating of the Tertiary volcanics in Lower Silesia, Poland. IV. Further K-Ar and paleomagnetic data from late Oligocene to early Miocene basaltic rocks of the Fore-Sudetic Block. *Annales Societatis Geologorum Poloniae*, 74, p. 1.

Birkenmajer K., Z. Pécskay, J. Grabowski, M.W. Lorenc, P. Zagożdżon. 2007. Radiometric dating of the Tertiary volcanics in Lower Silesia, Poland. V. K-Ar and palaeomagnetic data from late Oligocene to early Miocene basaltic rocks of the North-Sudetic Depression. *Annales Societatis Geologorum Poloniae*, 77, pp. 1–16.

Bonadiman C., M. Coltorti, L. Beccaluva, W.L. Griffin, S.Y. O'Reilly, F. Siena. 2011. Metasomatism versus host magma infiltration: A case study of Sal mantle xenoliths, Cape Verde Archipelago. *Geological Society of America Special Papers*, 478, pp. 283–305.

Coltorti M., L. Beccaluva, C. Bonadiman, L. Salvini, F. Siena. 2000. Glasses in mantle xenoliths as geochemical indicators of metasomatic agents. *Earth and Planetary Science Letters*, 183, pp. 303–320.

Dawson J.B. 2002. Metasomatism and partial melting in upper-mantle peridotite xenoliths from the Lashaine Volcano, Northern Tanzania. *Journal of Petrology*, 43, pp. 1749–1777.

Deer W.A., R.A. Howie, J. Zussman. 1993. *An Introduction to the Rock-Forming Minerals.* New York: Longman Scientific & Technical, pp. 1–696.

Dèzes P., S.M. Schmid, P.A. Ziegler. 2004. Evolution of the European cenozoic rift systems: Interaction of the Alpine and Pyrenean orogens with their foreland lithosphere. *Tectonophysics*, 389, pp. 1–33.

Griffin W.L., S.Y. O'Reilly, C.G. Ryan. 1999. *The Composition and Origin of Sub-continental Lithospheric Mantle.* Houston: The Geochemical Society Special Publications, pp. 13–45.

Higgins M.D. 2000. Measurement of crystal size distributions. *American Mineralogist*, 85, pp. 1105–1116.

Klügel A., Reactions between mantle xenoliths and host magma beneath La Palma (Canary Islands): Constraints on magma ascent rates and crustal reservoirs. *Contributions to Mineralogy and Petrology*, 131, pp. 237–257.

Ladenberger A. 2006. *Petrogenesis of Tertiary volcanic rocks from southwestern Poland.* PhD thesis, Jagiellonian University.

Le Maitre R.W., P. Bateman, A. Dudek, J. Keller, J. Lameyre, M.J. Le Bas, P.A. Sabine, R. Schmid, H. Sorensen, A. Streckeisen, A.R. Woolley, B. Zanettin. 1989. *A Classification of Igneous Rocks and Glossary of Terms: Recommendations of the International Union of Geological Sciences Subcommission on the Systematics of Igneous Rocks.* Oxford: Blackwell Scientific Publications, pp. 1–236.

Matusiak-Małek M. 2010. *Peridotitic xenoliths from the Cenozoic lavas of the Złotoryja, Jawor and Lądek Zdrój vicinities (Lower Silesia).* PhD thesis, University of Wrocław.

Matusiak-Małek M., J. Puziewicz, T. Ntaflos, M. Grégoire, H. Downes. 2010. Metasomatic effects in the litospheric mantle beneath the NE Bohemian Massif: A case study of Lutynia (SW Poland) peridotite xenoliths. *Lithos*, 117, pp. 49–60.

Mercier J.C.C., A. Nicolas. 1975. Textures and fabrics of upper–mantle peridotites as illustrated by xenoliths from basalts. *Journal of Petrology*, 16, pp. 454–487.

Meyer R., G.R. Foulger. 2007. *The European Cenozoic Volcanic Province Is Not Caused by Mantle Plumes*, www.mantleplumes.org.

Morimoto N. 1989. Nomenclature of pyroxenes. Subcomission of new minerals and mineral names. International mineralogical association. *Canadian Mineralogist*, 27, pp. 143–156.

Puziewicz J., J. Koepke, M. Grégoire, T. Ntaflos, M. Matusiak-Małek. 2011. Lithospheric mantle modification during cenozoic rifting in Central Europe: Evidence from the Księginki nephelinite (SW Poland) xenolith suite. *Journal of Petrology*, 53, pp. 2107–2145.

Shaw C.S.J. 1999. Dissolution of orthopyroxene in basanitic magma between 0.4 and 2 GPa: Further implications for the origin of Si-rich alkaline glass inclusions in mantle xenoliths. *Contributions to Mineralogy and Petrology*, 135, pp. 114–132.

Shaw C.S.J. 2009. Textural development of amphibole during breakdown reactions in a synthetic peridotite. *Lithos*, 110, pp. 215–228.

Shaw C.S.J., A. Klügel. 2002. The pressure and temperature conditions and timing of glass formation in mantle-derived xenoliths from Baarley, West Eifel, Germany: The case for amphibole breakdown, lava infiltration and mineral-melt reaction. *Mineralogy and Petrology*, 74, pp. 163–187.

Shaw C.S.J., Y. Thibault, A.D. Edgar, F.E. Lloyd. 1998. Mechanisms of orthopyroxene dissolution in silica-undersaturated melts at 1 atmosphere and implications for the origin of silica-rich glass in mantle xenoliths. *Contributions to Mineralogy and Petrology*, 132, s. 354–370.

Su B., H. Zhang, P. Sakyi, K. Qin, P. Liu, J. Ying, Y. Tang, S.K. Malaviarachchi, Y. Xiao, X. Zhao, Q. Mao, Y. Ma. 2010. Formation of melt pocket in mantle peridotite xenolith from western Qinling, Central China: Partial melting and metasomatism. *Journal of Earth Science*, 21, pp. 641–668.

Wierzchołowski B. 1993. Stanowisko systematyczne i geneza sudeckich skał wulkanicznych. *Archiwum Mineralogiczne*, 49, pp. 199–235.

Yaxley G.M., V. Kamenetsky. 1999. In situ origin for glass in mantle xenoliths from southeastern Australia: Insights from trace element compositions of glasses and metasomatic phases. *Earth and Planetary Science Letters*, 172, pp. 97–109.

Yaxley G.M., V. Kamenetsky, D.H. Green, T.J. Falloon. 1997. Glasses in mantle xenoliths from western Victoria, Australia, and their relevance to mantle processes. *Earth and Planetary Science Letters*, 148, pp. 433–446.

Yoder H.S., I. Kushiro. 1969. Melting of a hydrous phase: Phlogopite. *American Journal of Science*, 267-A, pp. 558–582.